Relationship between Activation Energy and Bottleneck Size for Li^+ Ion Conduction in NASICON Materials of Composition $LiMM'(PO_4)_3$; M, M′ = Ge, Ti, Sn, Hf

Ana Martínez-Juárez, Carlos Pecharromán, Juan E. Iglesias, and José M. Rojo*

Instituto Ciencia de Materiales de Madrid, Consejo Superior de Investigaciones Científicas (CSIC), Cantoblanco, 28049 Madrid, Spain

Received: October 10, 1997[⊗]

The activation energy involved in the motion of Li^+ ions along the conduction channels of the NASICON framework has been determined from electrical conductivity measurements in samples of composition $LiM_2(PO_4)_3$ and $LiMM'(PO_4)_3$, where M and M′ are Ge, Ti, Sn, and Hf, all compounds belonging to space group $R\bar{3}c$. Two lithium sites, M1 and M2, inside the channels, can be distinguished. The sites are connected through triangular bottlenecks of oxygen atoms, and the size of the bottleneck has been estimated from refined and simulated structures for each composition. The plot of activation energy vs bottleneck size shows two regimes: for sizes up to 2.04 Å the activation energy decreases steeply, but above 2.04 Å the activation energy is almost constant. These regimes are discussed on the basis of the effective Li^+ ionic radius for the compounds analyzed.

Introduction

Materials with NASICON structure are in general good ion conductors due to the presence of channels in which several ions such as Li^+, Na^+, and Ag^+ can move easily.[1,2] The relatively high ionic conductivity (10^{-4}−10^{-6} Ω^{-1} cm^{-1} at room temperature) and the negligible electronic conductivity are such that some of these materials are considered usable as solid electrolytes in lithium batteries. The NASICON framework is built up of MO_6 (M = Ge^{4+}, Ti^{4+}, Sc^{3+}, ...) octahedra and PO_4 tetrahedra sharing corners.[3] Two positions for the mobile ions can be distinguished:[2,4,5] one (M1) in an elongated octahedral oxygen environment at the intersection of three conduction channels, and the other (M2) in an 8−10 oxygen environment at each bend of the conduction channels. A scheme of the conduction channels including the two sites, M1 (open circles) and M2 (closed circles), which are arranged in an alternating manner, is shown in Figure 1, top. The bottleneck between both sites for the rhombohedral $R\bar{3}c$ symmetry is formed of three oxygen atoms whose centers make up an isosceles triangle (Figure 1, bottom). Six isosceles triangles which are the lateral faces of the oxygen antiprism around the M1 site are shown in Figure 1, bottom. In the absence of motion lithium is preferentially placed on M1 sites for rhombohedral phases of composition $LiM_2(PO_4)_3$, where M = Ge, Ti, and Hf.[6−8]

The ionic conductivity due to movement of Li^+ ions inside the channels seems to depend on the lattice parameters, whose values can be changed by choosing different chemical composition.[9−14] It has been observed that ionic conductivity is higher for materials with longer lattice parameters, and this fact has motivated preparation of NASICON compounds with larger octahedral cations. Despite the general agreement that Li^+ ion conduction can be improved in this way, controversy still remains about the underlying causes responsible for such improvement. The size of the cavities in which Li^+ resides, the size of the bottleneck, the strength of the Li−lattice oxygen bonds, and the increase in the number of Li^+ ions are some of the factors invoked to account for the increase in ionic conductivity.

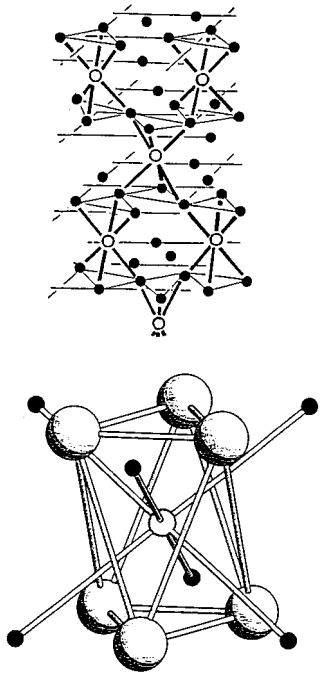

Figure 1. Top: Schematic representation of the conduction channels (thick lines) in the NASICON structure. The two sites for Li^+ ions are represented as follows: M1 by open circles, and M2 by closed circles. Bottom: Environment of the M1 site, and bottlenecks between M1 and M2 sites. Oxygen atoms are represented by the largest spheres, the M1 and M2 sites are represented by open and closed small spheres, respectively.

Another cause responsible for significant variations in Li^+ ion conduction is the phase transition observed in some compounds of NASICON structure. As an example, the ionic conductivity of $LiHf_2(PO_4)_3$ increases by 3 orders of magnitude when the triclinically distorted low-temperature phase is transformed into the rhombohedral $R\bar{3}c$ high-temperature phase.[15]

[⊗] Abstract published in *Advance ACS Abstracts,* December 15, 1997.

S1089-5647(97)03296-3 CCC: $15.00
Published on Web 01/08/1998

The aim of this work is to show that a relationship exists between the size of the bottleneck between the M1 and M2 sites and the activation energy involved in the motion of Li^+ ions along the conduction channels. A comparative study on NASICON materials, all of them with the same $R\bar{3}c$ space group but different composition ($LiMM'(PO_4)_3$; M,M′ = Ge, Ti, Sn, Hf), has consequently been undertaken.

Experimental Section

Samples of composition $LiM_2(PO_4)_3$, M = Ge, Ti, Sn, Hf, were prepared on the basis of a procedure described elsewhere.[16] Stoichiometric mixtures of Li_2CO_3, $(NH_4)_2HPO_4$, and the selected MO_2, M = Ge, Ti, Sn, Hf, were calcined at increasing temperatures in the range 180−1200 °C. The thermal treatments were cumulative, and the starting mixture was heated in each case at least at five different temperatures: 180, 300, 600, 800, and 1000−1200 °C. After each treatment the mixture was checked at room temperature by X-ray diffraction (PW-1710 Philips diffractometer with Cu Kα radiation). The products were considered pure phases when the characteristic X-ray peaks of the reagents and/or intermediate compounds such as pyrophosphates were not detected. Samples of composition $LiGeTi(PO_4)_3$, $LiGe_{0.5}Ti_{1.5}(PO_4)_3$, and $LiTiHf(PO_4)_3$ were also prepared by the same procedure, two oxides in the adequate proportion being used. In all cases the final product was a white powder sample.

Electrical measurements were carried out by the complex impedance method in the frequency range 10^{-1}−10^5 Hz on a 1174 Solartron frequency response analyzer coupled to a 1286 Solartron electrochemical interface. In some cases the measurements were carried out in the frequency range 10−10^7 Hz by using a 1260 Solartron impedance/gain-phase analyzer. The powder samples were pelletized and sintered at high temperature (1000−1200 °C); then, gold electrodes were deposited on the two faces of the pellets by vacuum evaporation. The impedance measurements were carried out in the range 20−200 °C, while the pellet was at steady temperature under nitrogen flow.

Results and Discussion

Ionic Conductivity. The impedance plot ($-Z''$ vs Z') recorded at 80 °C for a pellet of $LiGe_2(PO_4)_3$ composition, previously sintered at 1000 °C, is shown in Figure 2, top. Two arcs and an inclined spike are observed. The high-frequency arc, which is observed in the frequency range 10^3−10^5 Hz and shown in an expanded scale in the inset of that figure, is ascribed to the movement of Li^+ ions inside the grains (grain-interior response). The low-frequency arc appears in the range 1−10^3 Hz and is associated with the movement of the ions through the grain boundaries (grain-boundary response). The spike, which is observed in the range 0.2−1 Hz, is due to the blocking effect of the ions at the electrode surfaces (electrode response); this response is better observed at higher temperatures. Similar impedance plots were obtained for the other compositions. In all cases the presence of the grain-interior and grain-boundary response is consistent with the powder nature of the samples.

The real part of the conductivity, $\sigma'(\omega)$, related to the impedance through the expression

$$\sigma'(\omega) = Z'(\omega)/(Z'(\omega)^2 + Z''(\omega)^2)$$

is shown in Figure 2, bottom, as a function of angular frequency. Two plateaus, at low and high frequencies, associated with dc conductivities are observed. They differ at least by 1 order of magnitude and are ascribed as follows: the plateau at low

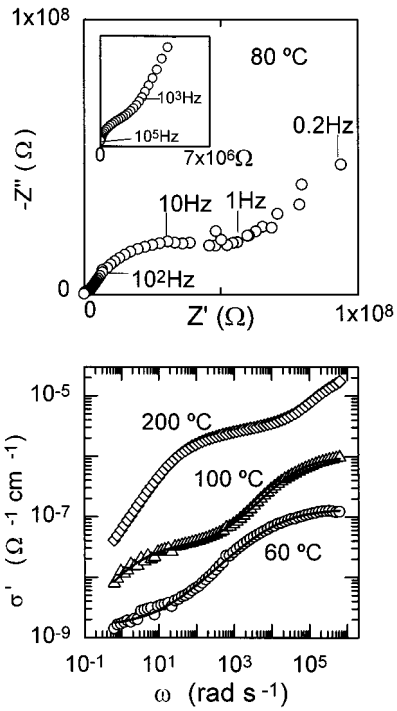

Figure 2. Top: Impedance plot obtained at 80 °C on a pellet of $LiGe_2(PO_4)_3$ previously sintered at 1000 °C. The inset shows the high-frequency arc in an expanded scale. Bottom: The real part of the conductivity vs angular frequency at different temperatures. The experimental data recorded at 60 and 100 °C are fitted to the expression $1/\sigma' = 1/\sigma'_{gb} + 1/\sigma'_{gi}$, where σ'_{gb} and σ'_{gi} stand for the grain-boundary and grain-interior conductivities, respectively. For these conductivities we adopted the form $\sigma_{dc} + A\omega^n$.

frequency to the grain-boundary dc conductivity, and that at high frequency to the grain-interior dc conductivity. Two dispersive regimes of the form ω^n, at low and high frequencies, are also observed. The experimental data fit the expression

$$1/\sigma' = 1/\sigma'_e + 1/\sigma'_{gb} + 1/\sigma'_{gi}$$

where σ', σ'_e, σ'_{gb}, and σ'_{gi} are the real conductivity for overall, electrode, grain-boundary, and grain-interior, respectively. The expression used for σ'_{gi} and σ'_{gb} is of the form $\sigma_{dc} + A\omega^n$, and for σ'_e is $A\omega^n$, where the term $A\omega^n$ accounts for the ac conductivity.[17,18] The solid lines in Figure 2, bottom, show the best fits to the already mentioned expression. Then, by this procedure, the dc conductivity corresponding to the grain-interior and grain-boundary response has been determined at each temperature for all the samples. Only the grain-interior dc conductivity is considered in this work.

The temperature dependence of the grain-interior dc conductivity is shown in Figure 3. The dc values were obtained on pellets which had been cold pressed and sintered at 1000−1200 °C. The density of the pellets was 80−95% of the density deduced from the unit cell volumes. The dc conductivity for the $LiSn_2(PO_4)_3$ sample is not included because a sintered pellet could not be prepared; the electrical measurements were done on a pellet of the composite formed of $LiSn_2(PO_4)_3$ and Teflon.[19] The experimental data shown in Figure 3 fit the Arrhenius equation

$$\sigma = \sigma_0 \exp(-E/kT)$$

where σ_0, E, and k are the pre-exponential factor, activation energy, and Boltzmann constant, respectively. The activation energy changes with chemical composition decreasing from 0.60

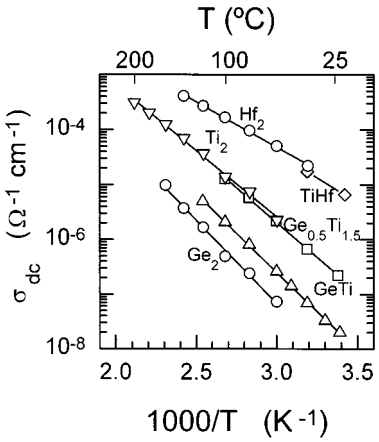

Figure 3. Plots of grain-interior dc conductivity vs 1000/*T* for the compositions $LiGe_2(PO_4)_3$ (○, Ge_2), $LiGeTi(PO_4)_3$ (Δ, GeTi), $LiGe_{0.5}Ti_{1.5}(PO_4)_3$ (□, $Ge_{0.5}Ti_{1.5}$), $LiTi_2(PO_4)_3$ (▽, Ti_2), $LiTiHf(PO_4)_3$ (◇, TiHf), and $LiHf_2(PO_4)_3$ (○, Hf_2). The full lines are the best fits to the expression $\sigma = \sigma_0 \exp(-E/kT)$.

eV for $LiGe_2(PO_4)_3$ to 0.33 eV for $LiHf_2(PO_4)_3$. A concomitant increase in conductivity is observed.

It is worth mentioning that the dc conductivity reported in this paper concerns exclusively the grain-interior response of samples of rhombohedral $R\bar{3}c$ symmetry. The dc conductivity at room temperature for $LiTi_2(PO_4)_3$ and $LiHf_2(PO_4)_3$ found by us (Figure 3) is almost coincident with the bulk values reported by some authors for the two rhombohedral phases.[14] However, a discrepancy exists for the values and the trend observed by other authors,[9,12] who reported higher conductivity for $LiTi_2(PO_4)_3$ than for $LiHf_2(PO_4)_3$. We have no explanation for it, although in these cases the dc conductivity measured seems to be the overall conductivity of the pellets, and the data would be affected by a significant contribution of grain-boundary dc conductivity. Values of dc conductivity differing by more than 1 order of magnitude and activation energies ranging 0.32−0.48 eV had been reported for the rhombohedral $LiHf_2(PO_4)_3$ phase, the differences found being accounted for by the relative contribution of grain-interior and grain-boundary dc conductivity to the overall dc conductivity.[20]

Bottleneck Size. The M1 site for Li^+ is surrounded by six oxygens in an antiprism (Figure 1, bottom), the site coinciding with the Wyckoff position 6b in the space group $R\bar{3}c$. Two kinds of faces can be distinguished: (i) the top and bottom faces, which are equilateral triangles, and (ii) the lateral faces, which are isosceles triangles. According to the model usually accepted for ionic conduction in the NASICON structure that Li^+ ions are moving along the conduction channels by hopping between the M1 and M2 sites, these ions should move through the lateral faces of the antiprism which, hence, operate as bottlenecks.

The sides of the isosceles triangles can be easily calculated from the oxygen coordinates and the lattice parameters when the crystal structure is known in detail,[7,21] i.e. for $LiGe_2(PO_4)_3$ and $LiHf_2(PO_4)_3$. In the case of $LiTi_2(PO_4)_3$ we have used the lattice parameters obtained from the powder X-ray pattern[12] and the coordinates reported[6] for $Li_{1+x}Ti_{2-x}In_x(PO_4)_3$, $x = 0.12$; this method assumes that the coordinates of the atoms have the same values in both structures because of the similar chemical composition of the two samples. For the other compositions, whose structures have not been refined yet, we have simulated their structures through DLS (distance least squares) calculations.[22,23] This method requires the lattice parameters and topology of the structure to be known; the symmetry operations are introduced as relations between specific atoms for which distances to other atoms are stipulated. The quantity to be minimized is

$$\rho = \sum_j w_j^2 (d_j^{\mathrm{p}} - d_j^{\mathrm{c}})^2$$

where the superscripts p and c stand for prescribed and calculated distances, w_j is the weight assigned to the *j*th distance, and summation is extended over all crystallographically independent distances. The quality of a solution can be assessed with the *R*-type index

$$R_{\mathrm{DLS}} = [\rho / \sum_j (w_j d_j^{\mathrm{p}})^2]^{1/2}$$

To check the validity of the DLS method for the NASICON structure, we have also applied this method to compositions whose structures are well refined, and we have compared the values deduced from DLS with those obtained from the refined structures.

In the NASICON structure of space group $R\bar{3}c$ there are 12 independent distances (2 P−O_T, 4 O_T−O_T, 2 M−O_O, and 4 O_O−O_O, where the subscript T stands for tetrahedral and O for octahedral) and 8 structural parameters (the *z*-coordinate of M, the *x*-coordinate of P, and all *x*,*y*,*z*-coordinates of both independent oxygen atoms) to determine. For the PO_4 tetrahedra, it is observed in refined structures that the P−O distances change very little from structure to structure, although two distances can be systematically distinguished: one shorter at 1.518 Å, and the other, 1.534 Å, both being the average value obtained from the data reported for different NASICON compounds.[1,3,5−7,21,24−28] These values were used as prescribed P−O distances in the DLS calculations we made. The O_T−O_T distances we prescribed were all 2.492 Å, which corresponds to a regular PO_4 tetrahedron whose P−O distance is 1.526 Å, the average of the two distances mentioned above. For the MO_6 octahedra there are also two M^{IV}−O distances reported in the literature,[1,3,5−7,21,24−28] whose difference on average is 0.04 Å. These arise from a small off-centering of the M^{IV} cation in the oxygen octahedron, the displacement being toward the inside of each $M_2(PO_4)_3$ group, i.e. the group formed of two MO_6 octahedra linked by three PO_4 tetrahedra. In addition, it is observed that the M−O distances reported for the resolved structures are 1−2% shorter than the values estimated for them from the "effective" radii of Shannon[29] for 6-fold coordination. Consequently we prescribed as average M−O distances those obtained from ref 29 after shrinkage of 1% and those were split into two types assuming a difference of 0.04 Å between these two types. The O_O−O_O distance prescribed was the distance corresponding to a regular octahedron having an M−O distance equal to the average M−O distance. For each composition 10 DLS calculations were made starting from atomic coordinates chosen at random with the above prescribed distances, and in all cases, the trial structures converged to NASICON-like structures with $R \approx 0.01$ or less.

Once the sides of the isosceles triangle were calculated from the refined and/or simulated structures, the radius of the circumscribed circumference was determined. This radius is taken hereafter as a measure of the bottleneck size, insofar as this distance minus the oxygen radius is the radius of the biggest sphere that can go through the bottleneck. The bottleneck size estimated for several compositions and the hexagonal lattice parameters used are outlined in Table 1. It is observed that the bottleneck size deduced from DLS-simulated structures is 1−3% larger than that deduced from refined structures; this can be due to the fact that only the covalent framework was considered in DLS calculations, while the real structures have Li^+ in the

TABLE 1: Hexagonal Lattice Parameters (a_H, c_H, Standard Deviations in Parentheses) and Bottleneck Sizes (d) As Calculated from Resolved Structures and DLS-Simulated Structures

sample	a_H (Å)	c_H (Å)	ref	d, structure (Å)	d, DLS (Å)
$LiGe_2(PO_4)_3$	8.275(5)	20.47(3)	7	1.943	1.968
$LiGeTi(PO_4)_3$	8.407(4)	20.583(8)	12		1.978
$LiGe_{0.5}Ti_{1.5}(PO_4)_3$	8.454(1)	20.694(7)	12		1.984
$LiTi_2(PO_4)_3$	8.509(2)	20.853(9)	6,12	1.986	2.008
$LiSn_2(PO_4)_3$	8.642(2)	21.574(7)	30		2.064
$LiTiHf(PO_4)_3$	8.66(2)	21.51(5)	11		2.12
$LiHf_2(PO_4)_3$	8.8306(1)	22.0270(5)	21	2.156	2.221

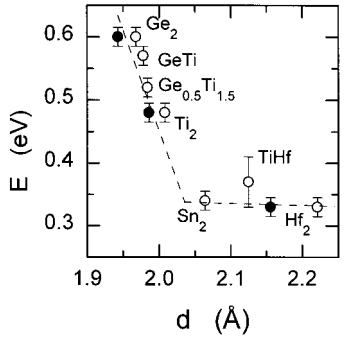

Figure 4. Activation energy (E) as deduced from grain-interior dc conductivity vs bottleneck size between M1 and M2 sites as estimated from refined structures (closed circles) and DLS-simulated structures (open circles) for the compositions $LiGe_2(PO_4)_3$ (Ge_2), $LiGeTi(PO_4)_3$ (GeTi), $LiGe_{0.5}Ti_{1.5}(PO_4)_3$ ($Ge_{0.5}Ti_{1.5}$), $LiTi_2(PO_4)_3$ (Ti_2), $LiSn_2(PO_4)_3$ (Sn_2), $LiTiHf(PO_4)_3$ (TiHf), and $LiHf_2(PO_4)_3$ (Hf_2). The dashed line is drawn to guide the eye. Vertical error bars are plotted.

M1 site, whose attraction on the oxygen anions tends to shrink the antiprism, thereby reducing the size of its lateral faces. The bottleneck size calculated from both refined and simulated structures becomes larger for longer lattice parameters.

Bottleneck Size−Activation Energy. Activation energy as deduced from electrical measurements vs bottleneck size as calculated from refined and simulated structures is shown in Figure 4. A steep decrease in activation energy, from 0.60 to 0.33 eV, for increasing bottleneck size between 1.90 and 2.04 Å is observed. Above 2.04 Å the activation energy decreases slightly, being almost constant. Then, there are two regimes clearly differentiated. Taking into account that the activation energy gives a measure of the hindrance in the movement of Li^+ ions along the conduction channels, we interpret the two observed regimes as follows: the size of the bottleneck is less than that of Li^+ ion in the first regime and larger in the second one. By assuming an oxygen radius of 1.40 Å, the subtraction of this value from that of the bottleneck crossover (2.04 Å) leads to a Li^+ radius of 0.64 Å, which can be considered as the effective ionic radius for Li^+ in the NASICON compounds analyzed. The value 0.64 Å for Li^+ is intermediate between the effective ionic radius reported[29] for a tetrahedral oxygen environment (0.59 Å) and for an octahedral oxygen environment (0.76 Å).

The activation energy in the second regime (0.33−0.35 eV) would be due to Li^+−lattice interaction. In fact, this value is close to that reported[31] (0.40 eV) for the compositions $Li_3Sc_{2-x}Al_x(PO_4)_3$, $x = 0.4-0.6$, which show also a NASICON structure but higher lithium content. The study of this point, however, will be the subject of further research.

Conclusions

The activation energy involved in the movement of Li^+ ions along the conduction channels of the NASICON framework is a parameter that includes at least two effects: one strongly dependent on the size of bottleneck between M1 and M2 sites, and the other related to lithium−lattice and/or lithium−lithium interactions.

Acknowledgment. Financial support by CICYT (Project MAT 95-0899) is gratefully acknowledged. C.P. thanks the Spanish Education and Culture Ministry for a contract under the mentioned project.

References and Notes

(1) Hong, H. Y.-P. *Mater. Res. Bull.* **1976**, *11*, 173.

(2) Goodenough, J. B.; Hong, H. Y.-P.; Kafalas, J. A. *Mater. Res. Bull.* **1976**, *11*, 203.

(3) Hagman, L.; Kierkegaard, P. *Acta Chem. Scand.* **1968**, *22*, 1822.

(4) Kohler, H.; Schulz H. *Mater. Res. Bull.* **1986**, *21*, 23.

(5) Petit, D.; Colomban, Ph.; Collin, G.; Boilot, J. P. *Mater. Res. Bull.* **1986**, *21*, 365.

(6) Tranqui, D.; Hamdoune, S.; Soubeyroux, J. L.; Prince, E. *J. Solid State Chem.* **1988**, *72*, 309.

(7) Alami, M.; Brochu, R.; Soubeyroux, J. L.; Gravereau, P.; Le Flem, G.; Hagenmuller, P. *J. Solid State Chem.* **1991**, *90*, 185.

(8) Paris, M. A.; Sanz, J. *Phys. Rev. B* **1997**, *55*, 14270.

(9) Subramanian, M. A.; Subramanian, R.; Clearfield, A. *Solid State Ionics* **1986**, *18−19*, 562.

(10) Alamo, J.; Roy, R. *J. Mater. Sci.* **1986**, *21*, 444.

(11) Chowdari, B. V. R.; Radhakrishnan, K.; Thomas, K. A.; Subba Rao, G. V. *Mater. Res. Bull.* **1989**, *24*, 221.

(12) Winand, J. M.; Rulmont, A.; Tarte, P. *J. Solid State Chem.* **1991**, *93*, 341.

(13) Aono, H.; Sugimoto, E.; Sadaoka, Y.; Imanaka, N.; Adachi, G. *J. Electrochem. Soc.* **1993**, *140*, 1827.

(14) Kuwano, J.; Sato, N.; Kato, M.; Takano, K. *Solid State Ionics* **1994**, *70−71*, 332.

(15) Paris, M. A.; Martinez-Juarez, A.; Iglesias, J. E.; Rojo, J. M.; Sanz, J. *Chem. Mater.* **1997**, *9*, 1430.

(16) Martinez, A.; Rojo, J. M.; Iglesias, J. E.; Sanz, J.; Rojas, R. M. *Chem. Mater.* **1994**, *6*, 1790.

(17) Jonscher, A. K. *Dielectric Relaxation in Solids*; Chelsea Dielectric Press: London, 1983.

(18) Reid, W. B.; West, A. R. *Solid State Ionics* **1991**, *45*, 239.

(19) Martinez-Juarez, A.; Jimenez, R.; Duran-Martin, P.; Ibañez, J.; Rojo, J. M. *J. Phys.: Condens. Matter* **1997**, *9*, 4119.

(20) Martinez-Juarez, A.; Iglesias, J. E.; Rojo, J. M. *Solid State Ionics* **1996**, *91*, 295.

(21) Losilla, E. R.; Aranda, M. A. G.; Martinez-Lara, M.; Bruque, S. *Chem. Mater.* **1997**, *9*, 1678.

(22) Meier, W. N.; Villiger, H. *Z. Kristallogr.* **1969**, *129*, 411.

(23) Baerlocher, C.; Hepp, A.; Meier, W. N. *DLS-76*, a program for the simulation of crystal structures by geometric refinement; Institut fur Kristallographie, ETH: Zurich 1976.

(24) Sljukic, M.; Matkovic, B.; Prodic, B. *Z. Kristallogr.* **1969**, *130*, 148.

(25) McCarron, E. M.; Calabrese, J. C.; Subramanian, M. A. *Mater. Res. Bull.* **1987**, *22*, 1421.

(26) Mbandza, A.; Bordes, E.; Courtine, P.; El Jazouli, A.; Soubeyroux, J. L.; Le Flem, G.; Hagenmuller, P. *React. Solids* **1988**, *5*, 315.

(27) Leclaire, A.; Borel, M. M.; Grandin, A.; Raveau, B. *Acta Crystallogr.* **1989**, *C45*, 699.

(28) Leclaire, A.; Borel, M. M.; Grandin, A.; Raveau, B. *Mater. Res. Bull.* **1991**, *26*, 207.

(29) Shannon, R. D. *Acta Crystallogr.* **1976**, *A32*, 751.

(30) Martinez-Juarez, A.; Rojo, J. M.; Iglesias, J. E.; Sanz, J. *Chem. Mater.* **1995**, *7*, 1857.

(31) Amatucci, G. G.; Safari, A.; Shokoohi, F. K.; Wilkens, B. J. *Solid State Ionics* **1993**, *60*, 357.